Many-body effects in highly *p*-type modulation-doped GaAs/$Al_xGa_{1-x}As$ quantum wells

S. Wongmanerod, B. E. Sernelius, P. O. Holtz, and B. Monemar
Department of Physics and Measurement Technology, Linköping University, S-581 83 Linköping, Sweden

O. Mauritz
Department of Physics, Royal Institute of Technology, S-100 44 Stockholm, Sweden

K. Reginski and M. Bugajski
Institute of Electron Technology, Al. Lotnikow 32/46, 02-668 Warsaw, Poland

(Received 18 October 1999)

Many-body effects have been optically investigated for modulation-doped quantum wells at high acceptor densities. The observed band-gap shrinkage, up to ≈ 20 meV, is consistent with calculations based on the Hartree and random-phase approximations including the finite well width effect. A recombination near the Fermi edge with light-hole character is strikingly enhanced at high acceptor densities. An interpretation based on carrier-carrier interaction is proposed. Finally, the exciton is found to be quenched for hole densities higher than $\approx 2\times 10^{12}$ cm^{-2}.

I. INTRODUCTION

In highly doped semiconductors, many-body interactions caused by the presence of a large number of carriers give rise to considerable modifications of the physical properties. The resulting exchange and correlation interactions induce a shrinkage of the fundamental band gap as well as higher subbands, the so-called band-gap renormalization (BGR).[1–4] The fundamental electron-hole interaction, such as the formation of excitons, is also affected at higher carrier concentrations. Due to the onset of many-body screening and the exclusion principle, the fundamental excitons become unstable at moderate densities and are quenched at higher concentrations. This is contrary to the Mahan-type exciton, the so-called Fermi-edge singularity[5–12] which has been reported to survive to high electron densities. So far, investigations on many-body effects in *p*-type modulation-doped quantum wells (MDQW's) have only been reported for acceptor concentrations up to moderate levels[2,13] where the observed many-body effects, e.g., the BGR, are comparable with the concentration dependence on the exciton energy. In this work, we report on many-body effects caused by high hole densities in *p*-type MDQW's at which the exciton energy variation is significantly smaller than the BGR, as observed in our optical spectra and compared with theoretical predictions on the many-body effects.

II. SAMPLES AND EXPERIMENTAL SETUP

The samples used in our study are symmetrically MDQW's grown by molecular-beam epitaxy. On top of a semi-insulating GaAs substrate and a GaAs buffer layer, 50 periods of 150-Å-wide undoped GaAs wells were sandwiched between 150-Å-thick $Al_{0.7}Ga_{0.3}As$ barriers, and finally a GaAs capping layer. In the center of each $Al_xGa_{1-x}As$ barrier, a 50-Å-thick Be-doped layer was grown. A series of samples was prepared with varying acceptor concentration together with an undoped reference sample. The hole sheet densities as derived from Hall-effect measurements are presented in Table I. For the photoluminescence (PL) and PL excitation (PLE) measurements, a tunable titanium-doped sapphire solid-state laser was used as an excitation source. The emitted light from the samples was detected by a 1-m double-grating monochromator and a cooled GaAs photomultiplier. For the polarization-dependent measurements we have employed the photoelastic modulation technique.

III. EXPERIMENTAL RESULTS AND DISCUSSION

The profound impact of many-body effects is illustrated by the development of the PL and PLE spectra with increasing hole concentration in Fig. 1. The PL spectra are dominated by the fundamental recombination between photoinduced electrons from the lowest conduction band and holes from the highest occupied two-dimensional (2D) heavy-hole (hh) subbands (labeled *A*). This peak exhibits a significant redshift as the hole concentration increases. The shift measures up to 20 meV for the sample with the highest acceptor doping (sample No. 196) relative to the undoped reference sample. The observed redshift is attributed to the BGR due to the exchange and correlation effects on the free carriers. However, this redshift is reduced with decreasing exciton binding energy, resulting in an increasing (exciton) recombination energy. As reported earlier, the oscillator strength of

TABLE I. Acceptor concentrations and estimated hole sheet concentrations.

Sample No.	N_a (cm^{-3})	p (cm^{-2})
Ref.	undoped	-
193	1×10^{18}	0.7×10^{12}
194	2×10^{18}	1.3×10^{12}
195	4×10^{18}	2.2×10^{12}
196	8×10^{18}	3.1×10^{12}

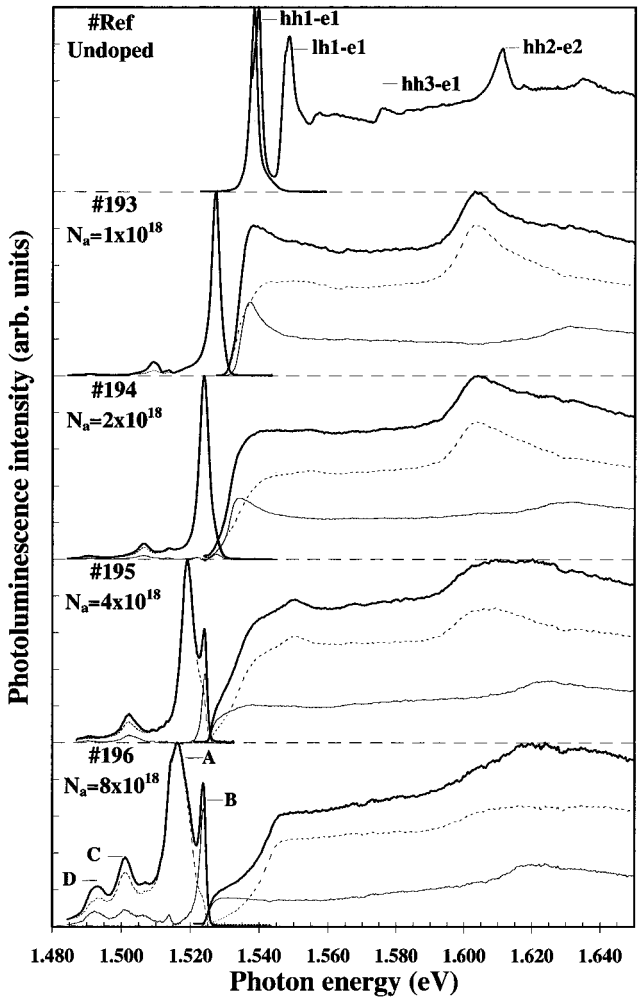

FIG. 1. The evolution of the PL and PLE spectra (thick lines) measured at 2 K with different acceptor concentrations $[N_a]$. The detections for the PLE were at the low-energy tail of the main PL emissions. The corresponding lh and hh contributions for the PL and PLE spectra are also displayed as $\sigma-$-polarized (thin lines) and $\sigma+$-polarized (broken lines) spectra, respectively.

the exciton drops rapidly, as the hole concentration exceeds 2×10^{11} cm^{-2}.[13] It is accordingly reasonable to assume that the excitonic effects are already essentially bleached in the main PL recombination in the low doped sample (No. 194). Consequently, it is in essence the BGR which is responsible for the PL shift at higher doping levels. For the samples with highest doping (Nos. 195 and 196), an enhanced recombination is observed on the very end of the high-energy tail as a separate, well-defined peak (labeled *B* in Fig. 1). As the temperature is raised, this peak is progressively smeared out and disappears completely at $\approx$25 K. From polarization-dependent PL measurements, demonstrated in Fig. 1, we find that peak *B* has a light hole (lh) character as illustrated by the negatively polarized ($\sigma-$) spectra. The interpretation of this peak will be further expounded upon below. The features labeled *C* and *D* in Fig. 1, displaying an obvious doping dependence, are interpreted as impurity-related recombinations in the QW, which will not be further discussed in this paper.

The PLE spectra are also significantly affected by an increasing carrier concentration. The hh- and lh-related PLE spectra, derived from polarization-dependent measurements ($\sigma+$ and $\sigma-$, respectively), exhibit a steplike feature as expected from a quasi-2D system. The low-energy cutoff edge for the $\sigma+$ (hh) PLE component, associated with the phase-space filling of the hh subbands is observed with an increasing energy separation, up to 30 meV, from the main PL peak. However, this behavior is not seen for the $\sigma-$ (lh) component, where instead a redshift of the low-energy cutoff edge due to the BGR is observed with a constant energy separation of 8–10 meV from the main PL peak. This fact indicates that the filling effect applies only to the hh subbands. The excitonic enhancement is evident in the PLE spectrum of the undoped reference sample with well-defined exciton peaks. As the acceptor concentration increases, the sharp excitonic peaks are smeared out, to finally disappear at high hole densities at which only steplike features remain.

Excitons related to unoccupied bands, such as lh1-$e1$ and hh2-$e2$, remain observable for acceptor concentrations up to 4×10^{18} cm^{-3} (corresponding to a sheet density of 2.2×10^{12} cm^{-2}) as can be seen for sample Nos. 193 and 194. This is similar to what was previously reported for *n*-type well-doped QW structures[14] but about one order of magnitude lower than for corresponding *p*-type structures.[15] For the occupied hh1 band, the related exciton is already quenched in the low-doped sample at an acceptor concentration below 1×10^{18} cm^{-3}. However, from our temperature-dependent measurements (not shown), this exciton is found to recover again at higher temperatures for every sample, e.g., above 40 K for sample No. 193. Huang *et al.*[13] observed a similar temperature dependence, and interpreted this thermal behavior for the exciton as a confirmation for the phase-space filling to be the important quenching mechanism.

To describe the many-body effects taking place in our structures quantitatively, we have performed calculations in order to theoretically predict the BGR for a comparison with our optical results. The computing was initialized by a self-consistent calculation on the valence-band structure within the multiband envelope-function approximation by using the Luttinger-Kohn 4×4 Hamiltonian[16] including the coupling between hh's and lh's together with the Poisson equation. In addition, the axial approximation was included, in which the Hamiltonian becomes invariant under rotation around the growth direction (along the z axis). The results achieved from the band dispersion relation for two of the samples with extremal doping conditions (Nos. 193 and 196) are depicted in Fig. 2. The subbands are labeled according to their wave-function properties at zero wave vector. Note the ordering of the subbands with hh character for the second subband and those with lh character for the next higher subband, which is a typical characteristic for wide wells. Subsequently, we make use of the valence-band structure previously derived together with the proper effective masses evaluated from this valence-band structure as an input for the BGR calculations.[3] In this way, the valence-band mixing and nonparabolicity, which otherwise give rise to a more narrow Fermi width than expected from a parabolic band with the effective mass valid at the band edge, are automatically included. The exchange-correlation energy leading to the BGR and lifetime broadening effects in the random-phase approximation are expressed as[1]

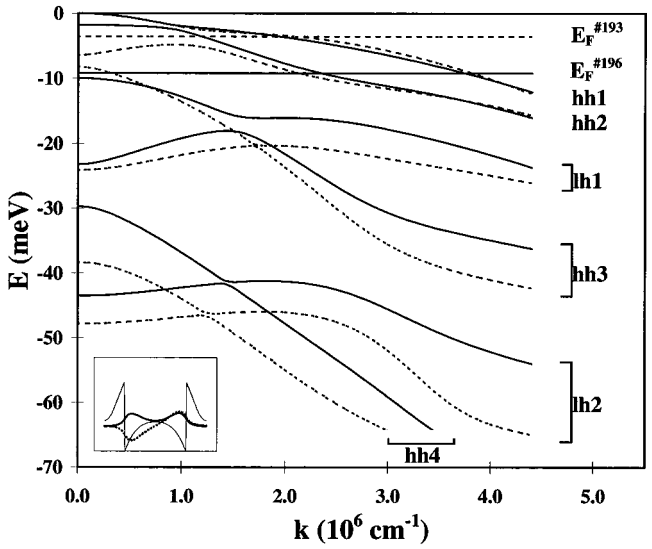

FIG. 2. A comparative plot of the dispersion curves for the hole band at two different hole densities calculated within the axial approximation. The broken and solid lines denote the results for the hole densities corresponding to the lowest (No. 193) and highest (No. 196) doping. The inset shows the results for the self-consistent potential of the valence band (thin line) and the hh1 (thick line) and the hh2 (dashed line) envelope functions for sample No. 196.

$$E_{xc} = -i\int_0^1 \frac{d\lambda}{\lambda}\frac{1}{2N} \times \sum_q{}' \left\{ \int_{-\infty}^{\infty}\frac{d\omega}{2\pi}\hbar\left[\frac{1}{1-\frac{\lambda\tilde{v}_q}{\kappa}\chi(q,\omega)}-1\right] - \frac{N\lambda\tilde{v}_q}{i\kappa}\right\}, \quad (1)$$

where N, κ, and $\chi(q,\omega)$ are the number of carriers, the background dielectric constant, the coupling constant, and the carrier susceptibility, respectively. Since we are dealing with QW of finite width and fairly high carrier concentrations, the matrix element for intralevel processes is not well represented by a strict 2D matrix element in which the finite extension of the wave function perpendicular to the well is neglected. Also, the validity of this approximation deteriorates as the momentum transfers for the important processes increase. In our earlier work[17] on QW with *p*-type doping inside the well, we found that the calculations based on a strict 2D approximation break down at high hole concentrations. Thus finite confinement is assumed in our case, and the tilde over the Coulomb interaction indicates that the strict 2D matrix elements have been modified to take this effect into account, according to[4]

$$\tilde{v}_q = C(q)v_q = C(q)\frac{2\pi e^2}{q}$$

$$C(q) = \int_{-W2}^{W2} dz \int_{-W2}^{W2} dz' |\varphi(z')|^2 e^{-q|z'-z|}|\varphi(z)|^2, \quad (2)$$

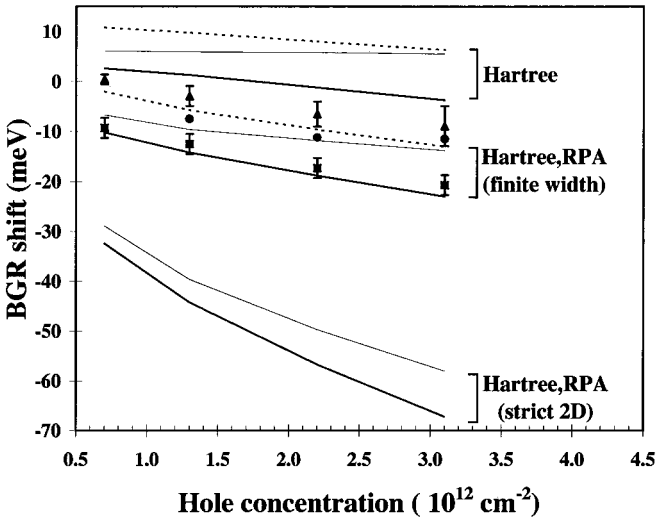

FIG. 3. The experimental results for the BGR shift of the $e1$-hh1$_{k=0}$ (squares), $e1$-hh1$_{k=k_F}$ (circles), and $e1$-lh1 (triangles) related transitions as a function of hole concentration. The thick lines, thin lines, and broken lines show the results of the calculations for the $e1$-hh1$_{k=0}$, $e1$-hh1$_{k=k_F}$, and $e1$-lh1 transitions with different theoretical approaches. ''Zero energy'' refers to the effective band gap obtained from the reference sample.

where W is the width of the well. The self-energy shifts have been derived within the Rayleigh-Schrödinger perturbation theory, where the shift of a state $\boldsymbol{k}$ is obtained as a variational derivative of the total interaction energy with respect to the occupation number for that state:

$$\Sigma_k = \frac{\delta(NE_{xc})}{\delta n_k}. \quad (3)$$

In Fig. 3, the numerical results on the BGR shifts for different approaches of the BGR are presented and compared with the experimental results in Fig. 1. It is clearly seen that the simple Hartree interaction has only a minor effect on the observed shift of the main PL band. The predominant contribution to the shift instead originates from the many-body self-energy shift (see Fig. 3). However, the strict 2D approximation overestimates the shift (by a factor of ≈ 3), while the approach based on the finite well width provides a closer agreement with the experimentally observed shift. Subsequently, these calculated results also show that the lh subband is not populated for all samples, as proposed above, and the lh subband experiences an exchange-correlation effect similar to the filled hh bands.

We turn our attention to the interpretation of peak *B*. The enhanced emission in the vicinity of the Fermi level is usually described in view of the Fermi-edge singularity (FES) with two possible conditions: The localization effect of free photogenerated carriers[5] and the carrier scattering between the Fermi edge and the next unoccupied lh subband.[6,7] However, we are dealing with the well-controlled GaAs/Al_xGa_{1-x}As system with limited interface roughness. Accordingly, the first condition is rarely fulfilled. Also the small effective electron mass in GaAs leads to a large recoil of the scattered electron and hence the destruction of the FES recombination.[8–10] The FES associated with the latter condition is unlikely to be observed, since the coupling of a FES

with virtual transitions to other hole subbands cannot be achieved in a QW system with a symmetric confined potential.[9,10] The experimental verifications of FES existing in similar systems are very rare; only weak features are observed in single QW,[11,12] where the symmetry is easily broken. Moreover, FES recombination is expected to maintain its hh character. Combining the above facts together with the lh character of peak *B* observable in polarization- dependent PL, the interpretation of peak *B* as FES recombination can be ruled out.

Our interpretation of peak *B* is based on an inspection of the valence-band structure (see Fig. 2). As the Fermi level approaches the lh band at higher hole concentrations (e.g., in sample Nos. 195 and 196), there is an efficient level broadening of the subbands arising from the carrier-carrier interaction, the so-called band-tail effect. This allows the lh band tail below the Fermi level to be partially populated and contribute to an enhanced recombination, observed as peak *B*. To confirm the interpretation, we introduce a theoretical modeling of the PL line shape using the approximation[1]

$$I(\Omega)\propto\int_{-\infty}^{\infty}\frac{d\omega}{(2\pi)^2}\int\frac{d^2k}{(2\pi)^2}n^e(\omega)A_k^e(\omega)\times n^h(\Omega-E_g-\omega)A_k^h(\Omega-E_g-\omega), \tag{4}$$

where $A(\omega)$ and $n(\omega)$ are the spectral function and the Fermi-Dirac occupation number, respectively:

$$\frac{A_k^i(\omega)}{2\pi}=\frac{1}{\pi}\frac{-\mathrm{Im}\,\Sigma^i(k)}{\{\omega-[\varepsilon_k^{i,0}\hbar+\mathrm{Re}\,\Sigma^i(k)]\}^2+[\mathrm{Im}\,\Sigma^i(k)]^2},$$
$$n^i(\omega)=\frac{1}{\exp\beta[\omega-\mu^i]+1},\quad i=e,h. \tag{5}$$

To calculate the PL line shape we need the self-energy shifts as derived previously, and the assumption of *k* conservation. The PL line-shape functions as obtained from Eq. (4) are compared with the experimental results in Fig. 4. As can be seen, the experimental data agree nicely with the theoretical predictions, indicating that our model, based on the band-tail effect alone can explain the appearance and PL line shape of peak *B*. We address the small deviation from the experimental results on the following facts: First we ignore effects of the valence-band anisotropy which is negligible for the BGR result but has to be taken into account for calculated line shape of peak *B*. Second, our line shape calculations rely on the assumption of *k* conservation. It has been theoretically demonstrated that the non-*k*-conserving processes, e.g., scattering via ionized impurities embedded in the barrier,[18] is also important for the PL line shapes. However, such processes can be regarded as small for these structures with thick spacers.

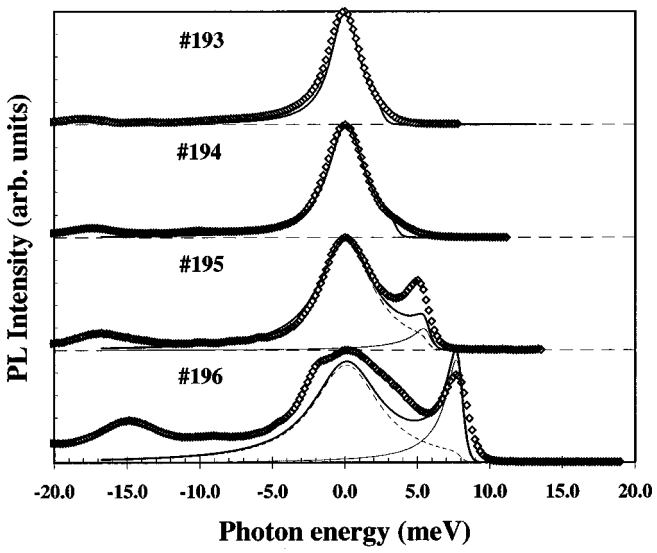

FIG. 4. Comparison of the fully calculated line-shape functions (thick lines) with the PL data (squares) as shown in Fig. 3. The calculated lh (thin lines) and hh (broken lines) contributions are also presented. The reference energy $E=0$ corresponds to the renormalized band gap as given in Fig. 3.

IV. CONCLUSIONS

We have investigated many-body effects in *p*-type modulation-doped QW for the high doping regime (up to 8×10^{18} cm^{-3}). A significant redshift of the optical spectra due to the band-gap renormalization has been observed and found to be in close agreement with our theoretical predictions. We also report on an observation of an enhanced recombination at the Fermi edge in *p*-type QW's, exhibiting light-hole character. Finally, the survival of excitons with increasing hole density has been studied. A striking difference for the survival of excitons between heavy and light-hole-related excitons is reported.

ACKNOWLEDGMENTS

S.W. gratefully acknowledges financial support from the Ministry of University Affairs, Thailand.

[1] B.E. Sernelius, Phys. Rev. B **34**, 5610 (1986).
[2] D.A. Kleinman and R.C. Miller, Phys. Rev. B **32**, 2266 (1985).
[3] P.A. Bobbert, H. Wieldraaijer, R. van der Weide, M. Kemerink, P.M. Koenraad, and J.H. Wolter, Phys. Rev. B **56**, 3664 (1997).
[4] O. Betbeder-Matibet, M. Combescot, and C. Tanguy, Phys. Rev. Lett. **72**, 4125 (1994).
[5] M.S. Skolnick, J.M. Rorison, K.J. Nash, D.J. Mowbray, P.R. Tapster, S.J. Bass, and A.D. Pitt, Phys. Rev. Lett. **58**, 2130 (1987).
[6] W. Chen, H. Fritze, A.V. Nurmikko, D. Ackley, C. Colvard, and H. Lee, Phys. Rev. Lett. **64**, 2434 (1990).
[7] W. Chen, M. Fritze, W. Walecki, A.V. Nurmikko, D. Ackley, J.M. Hong, and L.L. Chang, Phys. Rev. B **45**, 8464 (1992).
[8] P. Hawrylak, Phys. Rev. B **44**, 3821 (1991).
[9] F.J. Rodriguez and C. Tejedor, J. Phys.: Condens. Matter **8**, 1713 (1996).
[10] M. Kemerink, P.M.M. Thomassen, P.M. Koenraad, P.A. Bobbert, J.C.M Henning, and J.H. Wolter, Phys. Rev. B **58**, 1424 (1998).
[11] J. Wagner, P. Ganser, K. Köhler, A. Fischer, and K. Ploog, Surf. Sci. **263**, 628 (1992).
[12] D. Richards, J. Wagner, H. Schneider, G. Hendorfer, M. Mailer,

A. Fischer, and K. Ploog, Phys. Rev. B **47**, 9629 (1993).
[13] D. Huang, J.I. Chyi, and H. Morkoc, Phys. Rev. B **42**, 5147 (1990).
[14] C.I. Harris, B. Monemar, H. Kalt, and K. Köhler, Phys. Rev. B **48**, 4687 (1993).
[15] A.C. Ferreira, P.O. Holtz, B.E. Sernelius, A. Buyanov, B. Monemar, O. Mauritz, U. Ekenberg, M. Sundaram, K. Campman, J.L. Merz, and A.C. Gossard, Superlattices Microstruct. **18**, 153 (1995).
[16] J.M. Luttinger and W. Kohn, Phys. Rev. **97**, 869 (1955).
[17] P.O. Holtz, A.C. Ferreira, B.E. Sernelius, A. Buyanova, B. Monema, O. Mauritz, U. Ekenberg, M. Sundaram, K. Campman, J.L. Merz, and A.C. Gossard, Phys. Rev. B **58**, 4624 (1998).
[18] S.K. Lyo and E.D. Jones, Phys. Rev. B **38**, 4113 (1988).